

Effect of interfacial Cr on magnetoelectricity of Fe₂/CrO₂/BaTiO₃(001)

M. Hölzer,¹ M. Fechner,² S. Ostanin,² and I. Mertig^{2,1}

¹*Institut für Physik, Martin-Luther-Universität Halle-Wittenberg, D-06099 Halle, Germany*
²*Max-Planck-Institut für Mikrostrukturphysik, Weinberg 2, D-06120 Halle (Saale), Germany*
 (Dated: May 24, 2022)

On the basis of first-principles calculations we study the effect of interfacial Cr on the magnetoelectric properties of a composite multiferroic Fe_L/BaTiO₃(001), with the Fe thickness $L \leq 2$ monolayers. The use of the CrO₂-terminated interface instead of TiO₂ may significantly enhance magnetoelectricity in the system, showing an unexpected change in magnetization induced by the electric polarization reversal. In the case of $L = 2$, for instance, the magnetic order of the Fe bilayer can be switched from nearly zero ferrimagnetic to ferromagnetic upon polarization reversal.

PACS numbers: 31.15.Ae, 68.47.Gh, 73.20.At, 77.84.Lf, 77.80.Fm

I. INTRODUCTION

The occurrence of ferroelectricity and ferromagnetism in the same phase of a so called multiferroic¹ (MF) material allows both a switchable electric polarization, \mathbf{P} , and a switchable magnetization \mathbf{M} . More precisely, when an applied electric field displaces the magnetic ions of the multiferroic this affects the magnetic exchange coupling or, vice versa, the external magnetic field, \mathbf{H} , induces $P_i \sim \alpha_{ij} H_j$, where α_{ij} is the magnetoelectric (ME) tensor and $(i, j) = x, y, z$. When α is sufficiently strong this phenomenon may allow to store information in nanometer-sized memories with four logic states²⁻⁴.

The classification of multiferroics is based on different mechanisms of induced polarity⁵. The type-I class of multiferroics contains numerous perovskitelike materials in which \mathbf{P} appears at higher temperatures than magnetism. In these materials, \mathbf{P} and \mathbf{M} weakly interact with each other and, therefore, α is marginal there. In type-II MF, such as TbMnO₃, ferroelectricity is driven by the electronic order degrees related to a spin-orbit mechanism in conjunction mostly with the spin-spiral magnetic arrangement via the Dzyaloshinskii-Moria antisymmetric exchange. The latter creates $\mathbf{P} \sim \mathbf{r}_{ij} \times [\mathbf{S}_i \times \mathbf{S}_j]$, where \mathbf{r}_{ij} is the vector connecting neighboring spins \mathbf{S}_i and \mathbf{S}_j . Some of the type-II MFs may disclose a relatively large ME coupling. However, their ferroelectricity is caused by a particular type of magnetic order, which exists only at low temperature and which is predominantly antiferromagnetic.

Studies based on density functional theory (DFT) have significantly contributed to this rapidly developing field of multiferroics⁷. For instance, calculations from first-principles predict that the ME effect appears when a meV voltage is applied across the interface between the two unlike terminations, such as SrRuO₃/SrTiO₃⁸. The interface ME effect might be intrinsically enhanced by the use of material with high spin polarization. Indeed, a more robust scenario of magnetoelectricity occurs in epitaxially grown two-phase MF consisting of ferroelectric and ferromagnetic components. *Ab initio* calculations suggest that chemical bonding at the Fe/BaTiO₃(001)

interface is the source of strong ME coupling^{9,10}. Moreover, for the two opposite directions of \mathbf{P} (P_\downarrow and P_\uparrow), there are rather noticeable differences of $0.1-0.2\mu_B$ in the magnetic moments of interfacial Fe and Ti. This is a very promising phenomenon, which is entirely confined to the ferroelectric/ferromagnetic interface. The interface ME effect⁹ defines the change in \mathbf{M} at the coercive field E_c :

$$\mu_0 \Delta M \approx \alpha E_c. \quad (1)$$

For Fe/BaTiO₃(001), the estimated¹⁰ α of $\sim 2 \times 10^{-10}$ G cm²/V is two orders of magnitude larger than that predicted for SrRuO₃/SrTiO₃.

Currently, *ab initio* calculations which explore the trends and basic physics of magnetoelectrics, go ahead of experiment. For a single Fe monolayer (ML) on BaTiO₃(001), DFT predicts that perpendicular anisotropy is favored to in-plane anisotropy by 0.7 meV (0.5 meV) per Fe atom for P_\downarrow (P_\uparrow)¹⁰. Although the spin reorientation transition under switching of \mathbf{P} is not found from first principles, the ME coupling alters the magnetocrystalline anisotropy energy by $\sim 50\%$. The magnetic order of Fe/BaTiO₃ can be tuned by the Fe layer thickness to almost zero- \mathbf{M} ferrimagnetic upon deposition of a second Fe ML¹⁰. Ferromagnetic order is restored for the Fe films thicker than 3 ML where the shape anisotropy energy favors in-plane alignment of \mathbf{M} ¹¹. Epitaxial growth of the two-phase MF thin films of high quality continues to be very challenging. A 30-nm thick Fe(001) film has been grown recently on a ferroelectric BaTiO₃(001) substrate¹². For this composite MF, the trends of magnetic anisotropy are in good agreement with the corresponding *ab initio* calculations^{10,11}. Until recently, the DFT studies of the interface ME coupling were focused on chemically perfect films and superlattices with no impurities. Modeling the two different Fe₃O₄/TiO₂/BaTiO₃(001) interfaces, within the DFT, Niranjana *et al.*¹³ have found that ME coupling is stronger for the O-deficient type of the Fe₃O₄ interface. Therefore, the presence of extra oxygen or oxygen vacancies at the biferroic interface plays an important role. The effect of iron oxidation on the ME coupling of Fe/ATiO₃(001) ($A = \text{Ba, Pb}$) was simulated¹⁴ from first principles for oxygen coverages ranged between 0.5 and

2.0 adsorbed O atom per Fe atom. The calculations suggest that the magnetic properties of the Fe monolayer are gradually degraded with increasing O coverage. However, the change in magnetization which is induced by the \mathbf{P} reversal remains robust. Thus, the surface oxidation of composite MFs cannot destroy their potentially switchable magnetoelectricity.

It is well known that both the magnetic order of Fe-films and the related magnetic anisotropy are very sensitive to the presence of some other 3d elements. The alloying effect may result in important changes in magnetoelectricity and therefore, the DFT based modelling of chemical order in composite multiferroics would be useful. The effect of Fe-Co alloying on magnetoelectricity of thin-film Fe/BaTiO₃(001) has been studied recently¹⁵ from first principles using the coherent-potential approximation to DFT. It was found that the presence of >0.25 Co at.% per Fe atom stabilizes the ferromagnetic order in the two-ML thick and magnetically soft Fe-films. In this work, we investigate the ME coupling in the 1-ML and 2-ML thick Fe on BaTiO₃(001) (BTO), with a CrO₂ interfacial layer instead of TiO₂. Chromium dioxide (CrO₂) is an experimentally proven half metal, which shows a Curie temperature of 392 K and which possesses the largest spin polarization so far reported for this class of materials. As a consequence of the half-metallic feature of CrO₂, the occupied Cr 3d bands are fully spin polarized, leading to the spin moment of 2 μ_B per formula unit. Now we explore whether such a CrO₂-terminated interface of BTO enhances the ME coupling in Fe_L/BTO(001). In particular, for $L = 2$ we observe a dramatic change of magnetization in the topmost Fe ML under polarization reversal.

II. METHOD

To model the Fe_L/BaTiO₃(001) biferroic system within a slab geometry we used a 5-unit-cell (~ 2 -nm) thick BTO supercell covered by an Fe monolayer or Fe bilayer ($L = 1, 2$). A 2-nm-vacuum layer separates the slabs along [001]. For tetragonal BTO the equilibrium lattice parameters $a = 3.943$ Å and $c/a = 1.013$ were used. The Fe positions and atomic positions of the two top BTO unit cells were relaxed. In ferroelectric BTO, the cations and O of the alternating BaO and TiO₂ layers are displaced against each other in the [001] direction. This leads to spontaneous polarization along [001]. Here we model a dually polar ferroelectric. If the BTO cations are placed above O in the supercell then the negative intralayer displacements $\delta = (z_O - z_{cation}) < 0$ form the \mathbf{P} state pointing parallel to the surface normal (P_{\uparrow}) and, *vice versa*, the state P_{\downarrow} means that the $\delta > 0$. Before relaxation, the δ values of 0.082 Å and 0.086 Å were chosen in the TiO₂ and BaO layers, respectively¹⁶. The TiO₂-terminated type of the BTO interface was energetically preferred¹⁶. In this work, we substitute an interfacial Ti by Cr and added one or two ML of iron on the CrO₂-

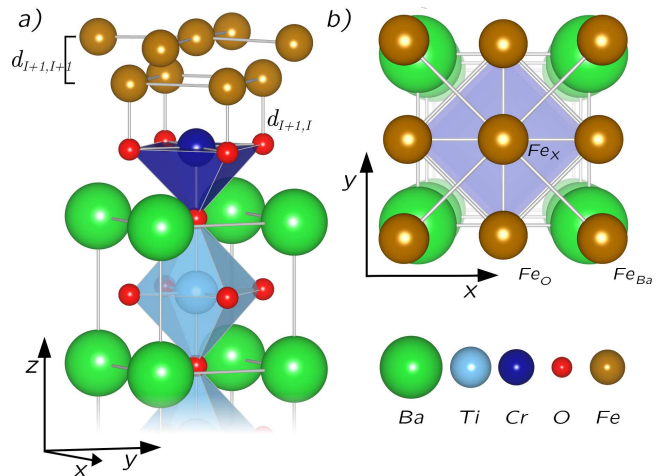


FIG. 1: Top layers of the $(\text{Fe}_2)_{L=2}/\text{CrO}_2/\text{BaTiO}_3(001)$ unit cell are shown as side- and top view in the panels (a) and (b), respectively. In panel (b), the interfacial Fe atoms above O are marked as “Fe_O” while the Fe atoms of the second ML, which sit above the perovskite cations are marked with the labels “Fe_{Ba}” and “Fe_X”.

terminated BTO(001). The Fe adatoms of the first ML relax atop oxygen¹⁰, while the Fe atoms of the second ML find their relaxed positions above the Ba and X=Cr sites. In Figure 1, we plot the side- and top view of relaxed Fe_L/CrO₂/BTO(001) for the case of $L = 2$. The positions of Fe above O, Ba and X are indicated by the corresponding labels in the panel (b).

In this DFT based study we used the Vienna *Ab initio* Simulation Package (VASP)^{17–19} within the local spin-density approximation. The electron-ion interactions were described by projector-augmented wave (PAW) pseudopotentials²⁰, and the electronic wave functions were represented by plane waves with a cutoff energy of 650 eV. For ionic relaxation the $8 \times 8 \times 4$ k-point Monkhorst-Pack²¹ mesh was used. The ionic relaxation was performed until the forces were less than 1×10^{-3} eV/Å. To calculate the electronic density of states (DOS) we used the $30 \times 30 \times 15$ k-point mesh. For each completely relaxed atomic configuration we performed the spin-polarized calculations starting from the ferromagnetic (FM) or, alternatively, from the antiferromagnetic (AFM) configuration in the Fe layers. The induced magnetization of the XO₂ interface was as well investigated.

III. RESULTS AND DISCUSSION

Much effort has been recently put to show that the electric field-induced reversal of \mathbf{P} is able to vary the easy direction of magnetization in magnetically soft Co_{0.9}Fe_{0.1}²² and Ni_{0.78}Fe_{0.22} permalloy²³ attached to thin film of multiferroic BiFeO₃ (BFO) or, alternatively, to a single crystal of BiFeO₃. There is a problem, how-

ever, to form a ferroelectric single domain in the (001) plane of BFO. As a result, the magnetization of permalloy could not be completely switched. We suggest that BTO is a more promising material for switching M by an electric field in the FM layer. In our study of the 1-ML-thick Fe-electrode material deposited on BTO(001) we find that the two systems: $\text{Fe}_{L=1}/\text{TiO}_2/\text{BTO}$ and $\text{Fe}_{L=1}/\text{CrO}_2/\text{BTO}$ are both ferromagnetically ordered, while the ME coupling coefficient increases from $\alpha = 2.1 \times 10^{-10} \text{ G cm}^2/\text{V}$ in $\text{Fe}_{L=1}/\text{TiO}_2/\text{BTO}$ to the value of $7.2 \times 10^{-10} \text{ G cm}^2/\text{V}$ at the CrO_2 interface. Eq.(1) was used to estimate α . In the case of Fe bilayer, the magnetic order changes dramatically. The $\text{Fe}_{L=2}/\text{TiO}_2/\text{BTO}$ system is almost zero- M ferrimagnetic for the both \mathbf{P} states. Contrarily, $\text{Fe}_{L=2}/\text{CrO}_2/\text{BTO}$ changes its magnetic order from AFM to FM when the substrate polarization is switched from P_\downarrow to P_\uparrow , resulting in a ME coupling coefficient of $\alpha = 6 \times 10^{-8} \text{ G cm}^2/\text{V}$. Below we concentrate mainly on the case of $L = 2$.

A. Structural relaxation

Figure 2 shows the perovskite intralayer displacement between oxygen and cations along [001], $\delta = z_{\text{O}} - z_{\text{cation}}$, obtained after relaxation of $\text{Fe}_L/\text{XO}_2/\text{BTO}(001)$ ($L = 1, 2$, $X=\text{Ti}, \text{Cr}$ and $\mathbf{P} = P_\downarrow, P_\uparrow$). The interfacial layer and layers beneath are denoted in Fig. 2 by I, I-1, I-2, etc. The asymmetry of δ seen between P_\downarrow and P_\uparrow for the layers I, I-1 and I-2 as well as the magnitude of δ , which gradually decreases towards the interface, both mimic the effect of the depolarizing field and its screening. It should be noted that the state P_\downarrow is energetically preferred compared to P_\uparrow . For that reason the depolarization effect is rather strong for P_\uparrow as shown in Fig.2. For P_\downarrow , the value of δ is stable beneath the interface, namely, between the layers I-1 and I-3 and, therefore, the reduction of δ becomes crucial at the interface only. It turns out that interfacial CrO_2 obeys marginal δ , which value decreases when the second Fe ML is added. For P_\uparrow , the effect of $X=\text{Cr}$ on δ is more pronounced. For instance, when $L = 2$ and $\mathbf{P} = P_\uparrow$ the presence of Cr changes the sign of δ in layer I.

In Figure 3, we plot the relaxed distances between interfacial Fe and O atoms of XO_2 ($X = \text{Ti}, \text{Cr}$). It has been previously found from first principles that the TiO_2 termination of $\text{BTO}(001)$ is energetically preferred¹⁶. When the first Fe ML is deposited on $\text{TiO}_2/\text{BTO}(001)$ the Fe atoms find their relaxed positions above O^{10} at the distance $d_{I+1,I} \approx 1.78 \text{ \AA}$ as shown in the left panel of Fig. 3. Thus, Fe and O form a strong and relatively short chemical bond at the interface. Our calculations demonstrate that $d_{I+1,I}$ may increase by $\sim 5\%$ when the second Fe ML is added. The polarization reversal shows no effect on $d_{I+1,I}$. For $L = 1$ and the CrO_2 -interface, we find that the corresponding $d_{I+1,I} \approx 1.7 \text{ \AA}$ is significantly reduced compared to the $\text{Fe}/\text{TiO}_2/\text{BTO}$ systems. When the Fe-(I+2) layer is added for $X=\text{Cr}$ and

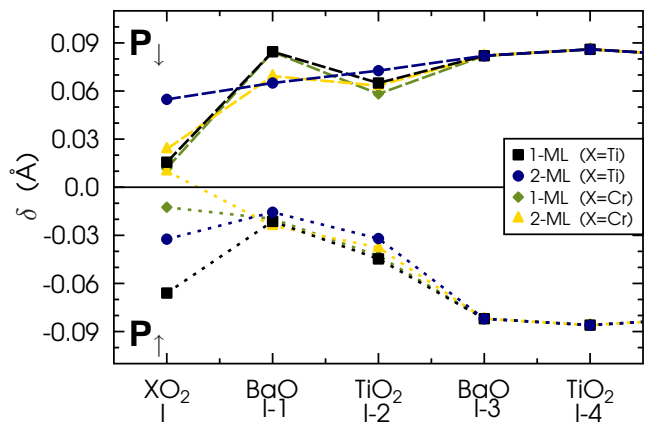


FIG. 2: Intralayer displacements $\delta = z_{\text{O}} - z_{\text{cation}}$ (in \AA) calculated for several top perovskite layers of $\text{Fe}_L/\text{XO}_2/\text{BaTiO}_3(001)$ ($L = 1, 2$, $X=\text{Ti}, \text{Cr}$ and $\mathbf{P} = P_\downarrow, P_\uparrow$). The interfacial layer and layers beneath are denoted by I, I-1, I-2, etc.

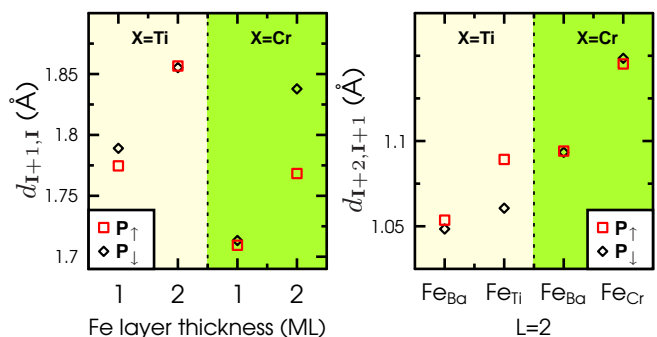


FIG. 3: Interlayer distances $d_{I+1,I}$ between the Fe adlayer I+1 and interfacial O are shown versus the Fe thickness $L = 1, 2$ in the left panel. For $L = 2$, the distances $d_{I+2,I+1}$ between the topmost $\text{Fe}_X/\text{Fe}_{Ba}$ sites and the Fe-(I+1) layer are shown in the right panel. Each system is dually polar.

P_\uparrow , the separation between Fe and O is increased to the corresponding $X=\text{Ti}$ value. For the opposite polarization P_\downarrow and $L = 2$, a $\sim 5\%$ -increase of $d_{I+1,I}$ was obtained. The latter result suggests a very promising scenario of magnetoelectricity in the $\text{Fe}_L/\text{CrO}_2/\text{BTO}$ system with $L = 2$. Since the Fe-(I+2) atoms of the second layer are inevitably placed above the perovskite cations, the corresponding Fe_X and Fe_{Ba} sites are nonequivalent as shown in Fig. 1. In Fig. 3(b) we plot the relaxed interlayer separation $d_{I+2,I+1}$ between the Fe layers I+2 and I+1 for the case of $L = 2$. In general, the presence of Cr at the interface makes $d_{I+2,I+1}$ larger compared to the reference $\text{Fe}_L/\text{TiO}_2/\text{BTO}$ system but, most importantly, $d_{I+2,I+1}$ is not changed upon \mathbf{P} reversal, except for a 3 %-increase at the Fe_{Ti} site.

B. Electronic and magnetic properties

Fig. 4 shows the site-projected DOS of paraelectric cubic BaTiO₃ together with the DOS of hypothetic cubic BaCrO₃. The two perovskites were calculated using the same lattice parameter $a = 3.943 \text{ \AA}$. For BTO we obtained an insulating band gap of $\sim 2 \text{ eV}$, which is typically underestimated within the local density approximation. The conduction band of BTO is formed mainly by the

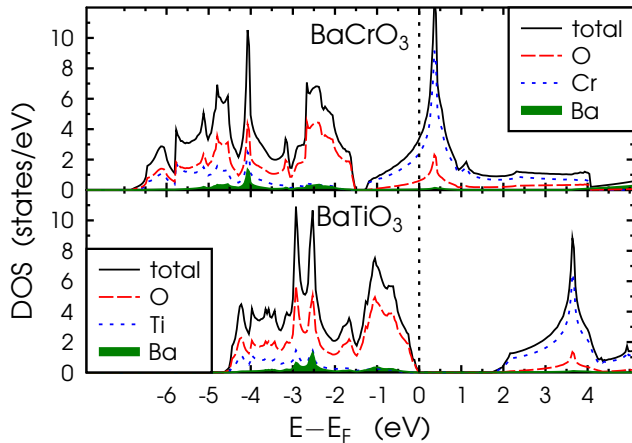


FIG. 4: The total and site-projected DOS of cubic BaTiO₃ and hypothetic BaCrO₃ calculated using the same lattice parameter $a = 3.943 \text{ \AA}$.

Ti 3d states whereas the upper valence band is largely composed by the O 2p states. In BaCrO₃, the DOS is typically metallic while the 3d states of Cr dominate near the Fermi level, E_F . There is a marginal pseudogap seen at -1.5 eV below E_F . Therefore, one can expect relatively strong metallization at the Fe/CrO₂ interface compared to Fe/TiO₂.

In Fe_{L=1}/TiO₂/BTO the FM order is energetically favorable against the AFM solution by 0.7 eV/cell (0.75 eV/cell) for P_\uparrow (P_\downarrow). Here, the Fe and O magnetic moments are aligned parallelly whereas the Ti magnetic moment, originating from hybridization of the Ti 3d and Fe 3d minority states⁹, is antiparallely aligned. All magnetic moments of the system are collected in Table I. The polarization reversal from P_\downarrow to P_\uparrow yields the magnetization change $|\Delta M| = 0.028 \mu_B/\text{cell}$ which formally results in the ME coupling of $2.1 \times 10^{-10} \text{ G cm}^2/\text{V}$. When Cr substitutes Ti at the interface, the lowest-energy configuration remains ferromagnetic. However, the negative magnetic moment of $\sim 2 \mu_B$, induced on Cr, is much larger than m_{Ti} . For interfacial oxygen the calculated magnetic moment is about $0.1 \mu_B$. This value as well as m_{Cr} are in a good agreement with the experimental data of bulk CrO₂²⁴. Due to the large and negative Cr magnetic moment, the total magnetization of the system Fe_{L=1}/CrO₂/BTO is reduced by $\approx 2 \mu_B$ in comparison to that of Fe_{L=1}/TiO₂/BTO. Although m_{Cr} is moderately changed by \mathbf{P} reversal the corresponding $|\Delta M|$ results

in $\alpha = 7.2 \times 10^{-10} \text{ G cm}^2/\text{V}$, which is three times larger than the ME effect of Fe_{L=1}/TiO₂/BTO.

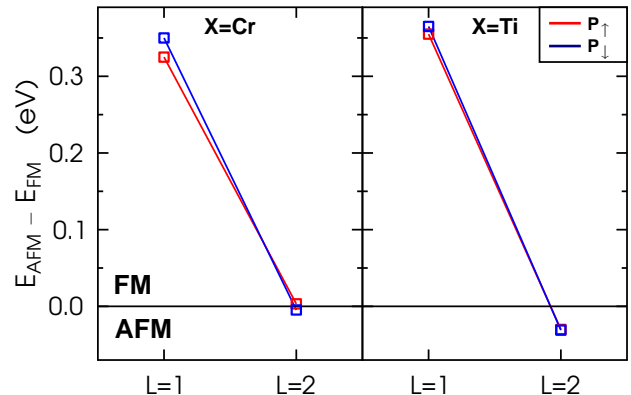


FIG. 5: Energy difference $\Delta E = E_{AFM} - E_{FM}$ between the AFM and FM configurations of Fe_L/XO₂/BTO ($X=\text{Cr, Ti}$ and $L = 1, 2$) is normalized per Fe atom.

The second Fe ML deposited on the TiO₂-terminated BTO(001) interface causes a specific case. There are two inequivalent I+2 sites situated atop Ba and Ti, respectively, which are labelled by Fe_{Ba} and Fe_X in Fig. 1. The different magnetic moments reflect the neighbourhood of these atoms such as their atomic volumes and hybridization of the electronic states. Let us consider, first, the case of X=Ti. The value of m_{Fe} in the layer I+1 is almost quenched while the two sizable moments in the surface layer I+2 are antiparallely aligned. This results in $M \rightarrow 0$ for Fe_{L=2}/TiO₂/BTO(001). In the case of the Fe bilayer on the CrO₂-terminated BTO, the lowest-energy configuration is antiferromagnetic for P_\downarrow and becomes ferromagnetic for P_\uparrow . For this polarization the Fe magnetic moments in the layer I+1 are far below their bulk value but the two Fe-(I+2) magnetic moments, which are ferromagnetically aligned to each other, contribute significantly to the total M . We estimate that the total magnetic moment of the system changes from $M < 0.3 \mu_B$ to $> 8 \mu_B$ per unit cell area upon polarization reversal. Thus, the polarization reversal produces for X=Cr the effect of switchable magnetization. In Fig. 5, the difference in energy, $\Delta E = E_{AFM} - E_{FM}$, calculated between the AFM and FM configurations and normalized per Fe atom, is plotted. For X=Cr the 2-ML-thick Fe film represents a specific case of a magnetically soft system at fixed \mathbf{P} . Nevertheless, any magnetic switch upon \mathbf{P} reversal requires an energy which exceeds the coercive field value of BTO.

To illustrate the interface ME coupling mechanism, we plot in Fig. 6 and Fig. 7 the spin density imbalance, $(n^+(\mathbf{r}) - n^-(\mathbf{r}))$, obtained under P -reversal near the interface of Fe_{L=2}/TiO₂/BTO and Fe_{L=2}/CrO₂/BTO, respectively. The (100) plane cutting through the X and O interfacial sites shows where the largest changes of the spin density occur and, hence, from where the

TABLE I: Local magnetic moments (in μ_B) calculated for the two Fe adlayers labeled by $I+1$ and $I+2$ and interfacial X ($X = \text{Cr}, \text{Ti}$) and O of $\text{Fe}_L/\text{XO}_2/\text{BaTiO}_3(001)$ ($L = 1, 2$). In the topmost Fe layer $I+2$, there are two nonequivalent sites denoted as Fe_{Ba} and Fe_{X} . The total magnetization M_{tot} includes the contributions from the interstitials. The energy difference between the AFM and FM configurations calculated for each system at $\mathbf{P} = (P_{\uparrow}, P_{\downarrow})$ is shown in eV per cell.

Site	Layer	$(\text{Fe}_2)_{L=1}/\text{CrO}_2/\text{BTO}$		$(\text{Fe}_2)_{L=2}/\text{CrO}_2/\text{BTO}$		$(\text{Fe}_2)_{L=1}/\text{TiO}_2/\text{BTO}$		$(\text{Fe}_2)_{L=2}/\text{TiO}_2/\text{BTO}$	
		P_{\uparrow}	P_{\downarrow}	P_{\uparrow}	P_{\downarrow}	P_{\uparrow}	P_{\downarrow}	P_{\uparrow}	P_{\downarrow}
Fe_{Ba}	(I+2)	—	—	+2.00	+2.24	—	—	+2.41	+2.36
Fe_{X}	(I+2)	—	—	+2.41	-2.61	—	—	-2.46	-2.36
Fe_{O}	(I+1)	+2.72	+2.75	+0.86	+0.44	+2.83	+2.81	-0.03	+0.00
X	(I)	-2.10	-2.00	+1.79	-0.11	-0.30	-0.22	0.00	+0.01
O	(I)	+0.10	+0.11	-0.03	0.00	+0.09	+0.08	-0.01	-0.01
$E_{\text{AFM}} - E_{\text{FM}}$ (eV)		+0.65	+0.70	+0.01	-0.02	+0.69	+0.75	-0.12	-0.12
M_{tot} (μ_B)		+3.86	+3.96	+8.28	+0.28	+5.87	+5.84	+0.02	-0.02
α ($\text{G cm}^2/\text{V}$)		7.20×10^{-10}		5.99×10^{-8}		2.08×10^{-10}		3.05×10^{-10}	

ME effect arises. Each of the four panels of Fig. 6–7 shows the local magnetization density calculated at fixed $\mathbf{P} = (P_{\downarrow}, P_{\uparrow})$. These are shown for the two possible magnetic configurations which are either FM or AFM. For $X=\text{Ti}$, both the P_{\uparrow} - and P_{\downarrow} -poled states are antiferromagnetically ordered, as shown in the panels (b) and (d) of Fig. 6. The two results are similar to each other. The largest negatively charged areas are seen around Fe_{X} - (I+2) while the n^+ - charged areas around the second Fe site of this layer are not shown in Fig. 6. All other sites of $\text{Fe}_{L=2}/\text{TiO}_2/\text{BTO}$ including Fe-(I+1) indicate very small magnetic moments. Inspecting the spin density imbalance seen in Fig.7(a) and Fig.7(d) for the two energetically preferred but oppositely poled configurations of $X=\text{Cr}$, we find many differences in the magnetic structure. The panel (a) shows the ferromagnetically ordered state P_{\uparrow} where the Fe and Cr atoms form rather spacious regions of positive spin density n^+ while n^- can be spotted around O, in the Fe interstitials and regions towards the surface. In the case of P_{\downarrow} , the energetically favorable AFM configuration, shown in the panel (d), is similar to that of $\text{Fe}_{L=2}/\text{TiO}_2/\text{BTO}$. Here, the large areas around Fe_{X} - (I+2) and also around interfacial Cr are negatively charged. Besides, the p_z -orbitals of interfacial O show their negative spin population resulting from hybridization with the $3d$ states of Fe-(I+1) whereas the O p_x and p_y orbitals, which form the bonds with the Cr $3d$ states, contribute to n^+ . Regarding the Fe-(I+1) atoms of $\text{Fe}_{L=2}/\text{CrO}_2/\text{BTO}$, Fig.7(d) shows that they contribute to n^+ contrarily to the case of $X=\text{Ti}$.

The site-projected and spin-resolved DOS calculated for $\text{Fe}_{L=2}/\text{XO}_2/\text{BTO}$ are plotted in the two panels of Fig. 8. For each system, the solid (shaded) lines represent the DOS curves in the P_{\uparrow} (P_{\downarrow}) state. The energetically preferable magnetic configurations are shown only in Fig. 8 for each direction of \mathbf{P} . In general, the DOS of the interfacial XO_2 layer is metallic for both systems. For $L = 2$ and $X=\text{Cr}$, however, the Cr $3d$ -DOS indicates relatively strong spin polarization at the Fermi level. This is not surprising since the DOS of hypothetical BaCrO_3 shows similar behavior, as shown in Fig. 4. When $X=\text{Ti}$, there is some insignificant presence of the Ti $3d$ states

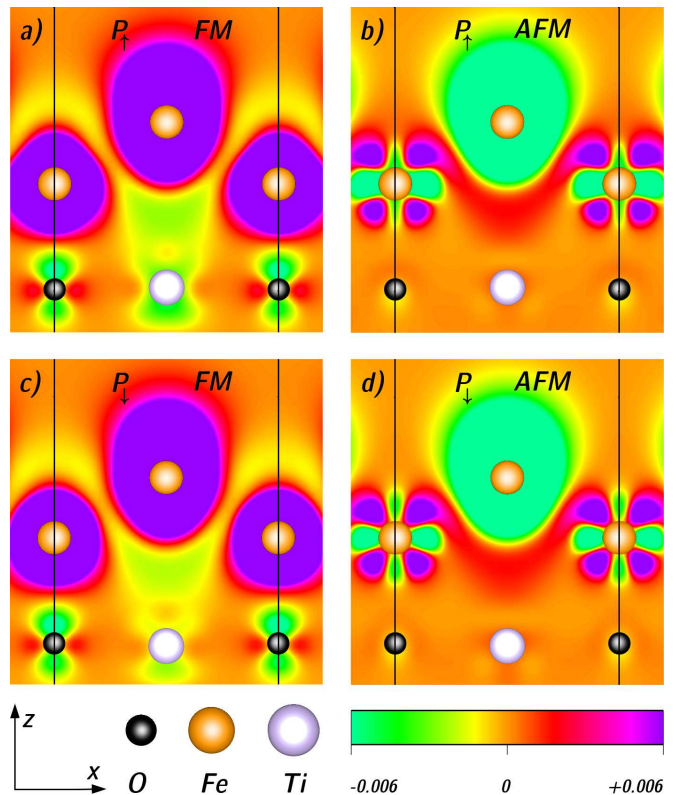


FIG. 6: Spin density imbalance $n^+(\mathbf{r}) - n^-(\mathbf{r})$ (in $e/\text{\AA}^{-3}$) within the (100) plane cutting through the Ti atoms of the $\text{Fe}_{L=2}/\text{TiO}_2/\text{BaTiO}_3(001)$ slab. The black vertical lines represent the unit cell boundary. The two top (bottom) panels show the polarization P_{\uparrow} (P_{\downarrow}). The panels (a) and (c) illustrate the FM ordering obtained for P_{\uparrow} and P_{\downarrow} , respectively, while the energetically preferable and nearly AFM configurations are shown in the panels (b) and (d).

in the BTO band gap below E_F , which entirely results from the hybridization with the Fe $3d$ states of the layer I+1. Another major difference in the DOS seen in Fig. 8 for $L = 2$ comes from the magnetic ordering of Fe_{X} . For $X=\text{Ti}$ the two Fe atoms in the topmost layer I+2

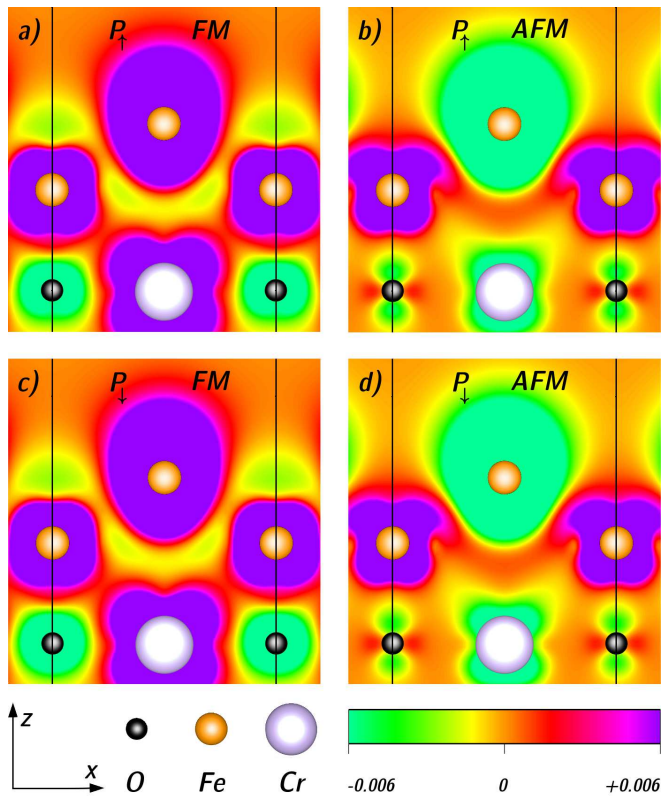


FIG. 7: Spin density imbalance (in $e/\text{\AA}^{-3}$) within the (100) plane cutting through the Cr atoms of $\text{Fe}_{L=2}/\text{CrO}_2/\text{BaTiO}_3(001)$. The two top (bottom) panels show the P_\uparrow (P_\downarrow) states while the left (right) panels illustrate the FM (AFM) ordering. For P_\uparrow (P_\downarrow), the lowest energy solution is the FM (AFM) configuration shown in ‘a’ (‘d’).

are coupled antiferromagnetically while the corresponding DOS curves show minor changes upon \mathbf{P} reversal. When $X=\text{Cr}$ the polarization reversal from P_\downarrow to the state P_\uparrow supports (i) the ferromagnetic order in the layer I+2, (ii) the relatively large magnetic moment $m(\text{Fe}_O) \sim 0.9 \mu_B$ in the layer I+1 and (iii) the $\sim 2\text{-}\mu_B$ change of m_{Cr} which is aligned parallelly to the Fe magnetic moments.

In Fig. 9, we plot the relative (in %) and absolute contributions (in μ_B) to $\Delta M = M(P_\downarrow) - M(P_\uparrow)$ coming from each magnetic species of $\text{Fe}_{L=2}/\text{XO}_2/\text{BTO}$. For the two biferroic interfaces studied here, the largest \mathbf{P} -induced change of \mathbf{M} comes from the Fe-(I+2) atoms. For $X=\text{Cr}$, however, the absolute value of ΔM approaches $\sim 7 \mu_B$ per unit cell. As result, the corresponding ME coupling coefficient increases significantly compared to that of $X=\text{Ti}$. We demonstrate that the case of $L=2$ and $X=\text{Cr}$ stabilizes the FM ordering in the system with \mathbf{P} pointing upwards. Surprisingly, this is completely due to rather modest 5% decrease of $d_{I+1,I}$ under \mathbf{P} reversal, as shown in Fig. 3. With decreasing $d_{I+1,I}$ above CrO_2 , the FM order is developing in the system. More precisely, when the Fe-(I+1) magnetic moment becomes larger ferromagnetism is stabilized in layer (I+2). In the case of $X=\text{Ti}$, the interlayer separations $d_{I+2,I+1}$ and $d_{I+1,I}$ are almost

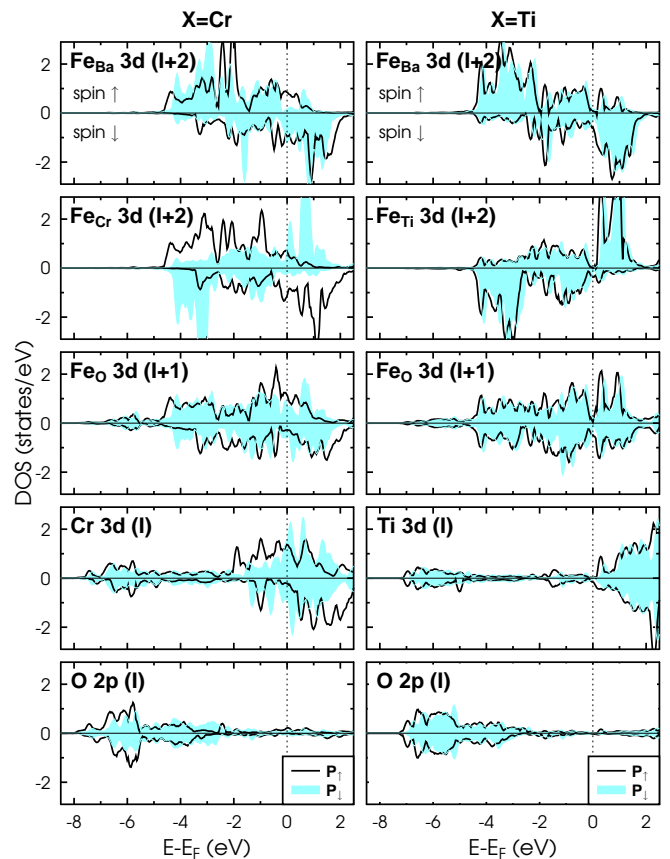


FIG. 8: Spin-polarized and site-projected DOS calculated for the metal 3d- and O 2p-states near the interface of $(\text{Fe}_2)_{L=2}/\text{CrO}_2/\text{BaTiO}_3(001)$ (left) and $(\text{Fe}_2)_{L=2}/\text{TiO}_2/\text{BaTiO}_3(001)$ (right). The two upper panels show the Fe 3d DOS of the surface layer I+2 while the Fe-I+1 DOS are shown in the middle panels. The 3d-DOS of interfacial cations Cr/Ti and oxygen 2p-DOS are plotted in the two lower panels. Solid lines and shaded areas represent the DOS for P_\uparrow and P_\downarrow , respectively.

the same upon the \mathbf{P} reversal that prevents any crucial spin reorientation in the topmost Fe ML.

IV. CONCLUSIONS

In summary, we present an *ab initio* study of the effect of interfacial Cr on the strength of magneto-electric coupling seen at the interface of multiferroic $\text{Fe}_L/\text{CrO}_2/\text{BaTiO}_3(001)$, with the Fe thickness $L \leq 2$ monolayers. We predict that a CrO_2 -terminated interface instead of TiO_2 may significantly enhance magneto-electricity in the system. The most attractive scenario is, however, obtained for the Fe bilayer where the magnetic order changes from nearly zero- \mathbf{M} ferrimagnetic to ferromagnetic upon polarization reversal in ferroelectric $\text{BaTiO}_3(001)$.

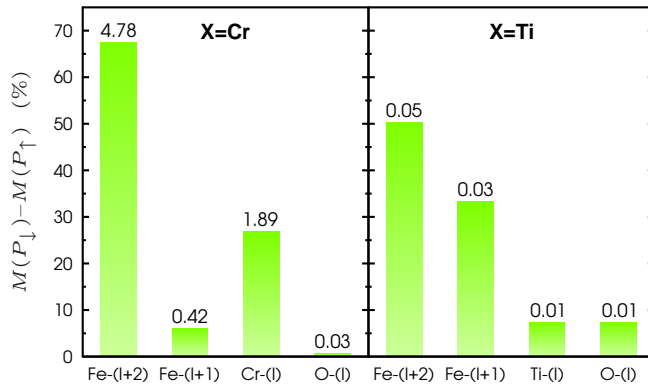


FIG. 9: Relative contributions (in %) of each magnetic species of $Fe_{L=2}/XO_2/BTO$ ($X = Ti, Cr$) to the magnetization change, ΔM , induced by polarization reversal. The contributions from the two Fe-(I+2) and two Fe-(I+1) atoms, one interfacial X and two O atoms were considered. The absolute values of ΔM are given (in μ_B) above each bar.

V. ACKNOWLEDGMENTS

This work was supported by the Collaborative Research Network SFB 762, 'Functionality of Oxidic Interfaces'. M. Fechner is a member of the International Max Planck Research School for Science and Technology of Nanostructures.

-
- ¹ K. F. Wang, J.-M. Liu, and Z. F. Ren, *Advances in Phys.* **58**, 321 (2009).
 - ² W. Eerenstein, M. Wiora, J. L. Prieto, J. F. Scott, and N. D. Mathur, *Nature Mater.* **6**, 348 (2007).
 - ³ S.-W. Cheong, *Nature Mater.* **6**, 927 (2007).
 - ⁴ F. Zavaliche, T. Zhao, H. Zheng, F. Straub, M. P. Cruz, P.-L. Yang, D. Hao, and R. Ramesh, *Nano Lett.* **7**, 1586 (2007).
 - ⁵ D. Khomskii, *Phys.* **2**, 20 (2009).
 - ⁶ M. Fiebig, *J. Phys. D: Appl. Phys.* **38**, R123 (2005).
 - ⁷ S. Picozzi and C. Ederer, *J. Phys.: Condens. Matter.* **21**, 303201 (2009).
 - ⁸ J. M. Rondinelli, M. Stengel, N. A. Spaldin, *Nat. Nanotechnol.* **3**, 46 (2008).
 - ⁹ C.-G. Duan, S. S. Jaswal, E. Y. Tsymbal, *Phys. Rev. Lett.*, **97**, 047201 (2006).
 - ¹⁰ M. Fechner, I. V. Maznichenko, S. Ostanin, A. Ernst, J. Henk, P. Bruno, I. Mertig, *Phys. Rev. B* **78**, 212406 (2008).
 - ¹¹ C.-G. Duan, J. P. Velev, R. F. Sabirianov, W. N. Mei, S. S. Jaswal, E. Y. Tsymbal, *Appl. Phys. Lett.* **92**, 122905 (2008).
 - ¹² C. Yu, M. Pechan, S. Srivastava, C. J. Palmstrom, M. Bielaszki, C. Brooks, D. Schlom, *J. Appl. Phys.* **103**, 07B108 (2008).
 - ¹³ M. K. Niranjana, J. P. Velev, C.-G. Duan, S. S. Jaswal, E. Y. Tsymbal, *Phys. Rev. B* **78**, 104405 (2008).
 - ¹⁴ M. Fechner, S. Ostanin and I. Mertig, *Phys. Rev. B* **80**, 094405 (2009).
 - ¹⁵ I.V. Maznichenko, M. Fechner, S. Ostanin, A. Ernst, J. Henk, I. Mertig, J.B. Staunton, unpublished.
 - ¹⁶ M. Fechner, S. Ostanin, I. Mertig, *Phys. Rev. B* **77**, 094112 (2008).
 - ¹⁷ G. Kresse and J. Hafner, *Phys. Rev. B* **49**, 14251 (1994).
 - ¹⁸ G. Kresse and J. Furthmüller, *Phys. Rev. B* **54**, 11169 (1996).
 - ¹⁹ J. Hafner, *J. Comput. Chem.* **29**, 2044 (2008).
 - ²⁰ G. Kresse and D. Joubert, *Phys. Rev. B* **59**, 1758 (1999).
 - ²¹ H. J. Monkhorst and J. D. Pack, *Phys. Rev. B* **13**, 5188 (1976).
 - ²² Y.-H. Chu, L. W. Martin, M. B. Holcomb, M. Gajek, S.-J. Han, Q. He, N. Balke, C.-H. Yang, D. Lee, W. Hu, Q. Zhan, P.-L. Yang, A. Fraile-rodriguez, A. Scholl, S. X. Wang, and R. Ramesh, *Nature Mat.* **7**, 478 (2008).
 - ²³ D. Lebeugle, D. Colson, A. Forget, M. Viret, A.M. Bataille and A. Gukasov, *Phys. Rev. Lett.* **100**, 227602 (2009).
 - ²⁴ D. J. Huang, H. T. Jeng, C. F. Chang, G. Y. Guo, J. Chen, W. P. Wu, S. C. Chung, S. G. Shyu, C. C. Wu, H. J. Lin, C. T. Chen, *Phys. Rev. B* **66**, 174440 (2002).